Elucidation of Interactions between Metal Ions and Ca Alginate-Based Ion-Exchange Resin by Spectroscopic Analysis and Modeling Simulation

ARTICLE *in* LANGMUIR · OCTOBER 2002

Impact Factor: 4.46 · DOI: 10.1021/la026060v

4 AUTHORS, INCLUDING:

Jiaping Paul Chen
National University of Singapore
137 PUBLICATIONS **4,476** CITATIONS
SEE PROFILE

Liang Hong
National University of Singapore
136 PUBLICATIONS **3,307** CITATIONS
SEE PROFILE

Shunnian wu
Nanyang Technological University
21 PUBLICATIONS **929** CITATIONS
SEE PROFILE

Elucidation of Interactions between Metal Ions and Ca Alginate-Based Ion-Exchange Resin by Spectroscopic Analysis and Modeling Simulation

J. Paul Chen,* Liang Hong, Shunnian Wu, and Lin Wang

Department of Chemical and Environmental Engineering, National University of Singapore, 10 Kent Ridge Crescent, Singapore 119260

Received June 12, 2002. In Final Form: September 19, 2002

In this study, a cost-effective calcium alginate-based ion-exchange resin (CABIER) was employed for treatment of metal waste streams. pH, concentration, and presence of competitive metal ions played important roles in the removal. The X-ray photoelectron spectroscopy (XPS) and Fourier transform infrared spectroscopy (FT-IR) analysis indicated that the functional groups on the carbohydrate backbone (i.e., C−O−R and COO^{-1}) were responsible for the binding of metals. It was found that the lead abstraction was driven by the ion exchange between Ca^{2+} and Pb^{2+}. On the contrary, the Cu^{2+} ion was stripped via both ion exchange with Ca^{2+} and coordination of the other functional groups. A new mathematical model based on ion exchange (between metal and calcium) and elementary coordination (among metals and functional groups) reactions successfully described and predicted the metal removal under various conditions (e.g., pH, concentration, and existence of competitive metal ions). It was found from the modeling that metal binding follows a decreasing order of $Pb^{2+} > Cu^{2+} > Ca^{2+}$.

Introduction

Metals are known to be essential for almost all kinds of living organisms.[1] When the concentrations exceed certain limits, the metals can become toxic and harmful to the living organisms. For this reason, the environmental pollution control authorities have imposed a tight control on the discharge of wastewater containing heavy metals from industries to watercourses.

Precipitation, ion exchange, adsorption, membrane technology, reduction, and many other novel methods are employed for metal treatment and recovery.[2−15] In particular, the application of nonliving organisms and their derivatives as biosorbents for heavy metal removal has been regarded as a potential approach.[3−11] These biosorbents come from different sources, including the cultivation and the byproducts of industrial fermentation.[3,5] It has been reported that they exhibit tremendous metal binding capacities.

As the organisms are cumbersome to use, the application of biopolymers extracted from metal-binding organisms has attracted much more attention. The calcium alginate-based ion-exchange resin (CABIER) was an example of such biopolymers that was developed in our previous study.[7,8] The CABIER can be prepared using a commercially available sodium alginate, which is a high-molecular-weight biopolymer. This resin has exhibited extremely high capacities and kinetics of binding heavy metal ions, and has shown to be rather stable under various chemical and physical conditions (e.g., pH and mixing strength).[8] Parameters that can affect the biosorption processes include pH, metal concentration, and presence of competing ions.

The chemical interaction between the CABIER and metal ions, however, was not studied in detail. Mathematical modeling could actually be used to elucidate the mechanisms of the metal binding onto the CABIER pellets. Spectroscopic approaches such as X-ray photoelectron spectroscopy (XPS) and Fourier transform infrared spectroscopy (FT-IR) can be applied to identify the functional groups in biosorbents. The measurements can provide information on chemical interactions, such as ion exchange, adsorption and redox reactions.

Some successful modeling studies are available in the literature to explain the metal biosorption or interaction between metal and organic ligands of various biosorbents (e.g., seaweeds).[5,10−14,16,17] A series of adsorption reactions among functional groups, hydrogen, and metal ions is considered, but the models normally do not include precipitation and aqueous reactions. A model with a consideration of surface complex formation (between functional groups and metals) was applied to interpret the experimental observations in copper and cobalt biosorption onto seafood process waste sludge.[5] A uniform functional group was used to represent hydroxyl, carboxyl,

* Corresponding author. Tel: +65-6874-8092. Fax: +65-6779-1936. E-mail: checjp@nus.edu.sg.

(1) Harvey, B. *Pediatrics* **1994**, *93*, 201−204.
(2) Chen, J. P.; Yu, H. J. *Environ. Sci. Health* **2000**, *A35*, 817−835.
(3) Volesky, B. *Biosorption of Heavy Metals*; CRC Press: Boca Raton, FL, 1989.
(4) Loaec, M.; Olier, R.; Guezennec, J. *Water Res.* **1997**, *31*, 1171−1179.
(5) Lee, S. M.; Davis, A. P. *Water Res.* **2001**, *35*, 534−540.
(6) Gin, K. Y. H.; Tang, Y. Z.; Aziz, M. A. *Water Res.* **2001**, *36*, 1313−1323.
(7) Chen, J. P.; Peng, J. *Adv. Environ. Res.* **1999**, *3*, 439−449.
(8) Chen, J. P.; Wang, L. *Sep. Sci. Technol.* **2001**, *36*, 16.
(9) Jang, L. K.; Geesey, G. G.; Lopez, S. L.; Eastman, S. L.; Wichlacz, P. L. *Water Res.* **1990**, *24*, 889−897.
(10) Schiewer, S.; Wong, M. H. *Environ. Sci. Technol.* **1999**, *33*, 3821−3828.
(11) Schiewer, S.; Volesky, B. *Environ. Sci. Technol.* **1995**, *29*, 3049−3058.
(12) Cernik M.; Borkovec, M.; Westall, J. C. *Langmuir* **1996**, *12*, 6127−6137.
(13) Vulava, V. M.; Kretzschmar, R.; Rusch, U.; Grolimund, D.; Westall, J. C.; Borkovec, M. *Environ. Sci. Technol.* **2000**, *34*, 2149−2155.
(14) Yiacoumi, S.; Tien, C. *Kinetics of Metal Ion Adsorption from Aqueous Solutions: Models, Algorithms and Applications*; Kluwer Academic Publishers: Norwell, MA, 1995.
(15) Chen, J. P.; Lin, M. S. *Water Res.* **2001**, *35*, 2385−2394.
(16) Yang, J.; Volesky, B. *Environ. Sci. Technol.* **1999**, *33*, 4079−4085.
(17) Esposito, A.; Pagnanelli, F.; Veglio, F. *Chem. Eng. Sci.* **2002**, *57*, 307−313.

10.1021/la026060v CCC: $22.00
Published on Web 10/25/2002

amino, and other groups. In a recent research study by Gin et al.,[6] a thermodynamics approach was utilized to describe the adsorption behavior by algae.

However, only a few equilibrium models have been developed for the metal uptake processes by alginate compounds. Jang et al.[9] employed an extended Langmuir isotherm to model metal removal by alginate gels in a batch loop fluidized bed reactor. They proposed that metal ion uptake was due to a chemical reaction between metal ions and carboxyl group.

Having a comprehensive understanding of the metal ion interaction with the CABIER is essential in order to control the process. So far, the relationship between the adsorption phenomenon and the chemical structure was not well investigated. In our previous study,[7,8] a conceptual model based on an ion-exchange mechanism was proposed based on macroscopic observations (i.e., measurement of the metal concentration difference); however, a mathematical model to accurately describe the removal capacities was not developed then.

In this study, we attempted to investigate the removal mechanisms through a series of instrumental analysis, such as XPS, FT-IR, and scanning electron microscopy (SEM). We then developed a mathematical model based on ion exchange and complexation principles to describe the removal phenomenon. A linkage of the spectroscopic investigations and the mathematical modeling was then established to help us better understand the process.

Materials and Methods

Materials. The CABIER was prepared by dispersing powdery sodium alginate (Fluka, Switzerland) into a stirred $CaCl_2$ solution. Other preparation procedures of the CABIER and some of its physical and chemical properties were documented in our previous papers.[7,8] Chemicals of analytical grades and basic equipment were the same as reported.[8]

Potentiometric Titration. To determine the ion-exchange properties of the resin, a series of titration experiments was carried out under two ionic strength values of 0.05 and 0.1 M. An amount of 0.5 g of resin was added to conical flasks containing 100 mL of 0.05 M $NaNO_3$ solution. After 24 h of stabilization, an acid-titration experiment was carried out by using 0.1 M HNO_3 solution. The titration experiment was repeated with an ionic strength of 0.1 M ($NaNO_3$).

Batch Equilibrium Adsorption Experiment. Lead and copper solutions were used to represent the metal-contaminated streams. In the equilibrium experiments to study the pH effect, $Pb(NO_3)_2$ and $Cu(NO_3)_2$ solutions with various initial pH values were prepared. The resins were added into the conical flasks containing the metal solutions. The flasks were placed in a shaking water bath with the temperature controlled at 25 °C for 2 d. The metal concentrations were measured by an inductively couple plasma emission spectroscopy (ICP-ES) (Perkin-Elmer Optima 3000).

In the isotherm experiments, the solution pH was controlled between 5.5 and 7, because the pH effect in this range is ignorable.[7,8] Various amounts of resins were added into the solutions of the same metal concentrations. All bottles were gently shaken at 25 °C for an equilibrium time of 2 d. The initial and final metal concentrations were determined by the ICP-ES. Competitive adsorption experiments were also conducted using similar procedures.

Scanning Electron Microscopy. The surface morphology of the resins was visualized by a scanning electronic microscope (JEOL, JSM-5600V, Japan). The SEM enables the direct observation of the surface microstructures of the fresh and used resins. Energy dispersive spectroscopy (EDS) with the SEM was also used to determine the chemical composition of the resins before and after copper uptake.

X-ray Photoelectron Spectroscopy. X-ray photoelectron spectroscopy (Kratos XPS System−AXIS His-165 Ultra, Shimadzu, Japan) was applied to determine the interactions between the organic functional groups in the resins and the metals of the following: (a) fresh CABIER, (b) Na alginate powder, (c) lead-adsorbed resins, (d) copper-adsorbed resins, and (e) the acid-titrated resins. Since the fresh CABIER was prepared by the sodium alginate and calcium chloride, its material composition could be characterized by C, O, and Ca. In addition, analysis for Pb and Cu was performed for the metal-adsorbed resins.

The XPS spectra were obtained by applying the energy source of monochromatic Mg Kα radiation (1253.6 eV) operated at 15 kV and 10 mA. The residual pressure in the analysis-chamber was 5×10^{-8} Pa. The wide scans were conducted from 0 to 1200 eV with a pass energy of 80 eV. The elements, C, O, Ca, Pb, and Cu, were scanned over the energy range of 282−294, 528−540, 344−360, 133−153, and 928−960 eV, respectively, with the pass energy of 40 eV. The aforementioned 5 kinds of samples were analyzed. The spectra were decoded using the curve-fitting program with the subtraction of Shirley background and the ratio of Gaussian (0)-Lorentzian (100%). For calibration purposes, the binding energy of the spectra was performed with the C 1s peak at 284.5 eV. When comparing the results with the reference, peaks were identified as the same if the difference of the peak position is within 0.5 eV.

Fourier Transform Infrared Spectroscopy. FT-IR spectroscopy was used to detest the vibration frequency changes in the resins. The spectra were collected by a FTS-135 (Bio-Rad) spectrometer within the range of 400−4000 cm^{-1} using a KBr window. The background obtained from the scan of pure KBr was automatically subtracted from the sample spectra. All spectra were plotted using the same scale on the absorbance axis.

Theoretical

Formulation of the Model. Alginate is a polysaccharide-like polymer containing three different functional groups: $-COO^-$ (carboxylate), $-C-O-C-$ (ether) and $-OH$ (alcohol). In the following modeling study, it was assumed that there was one generalized type of functional group (represented as R^{2-}) in the metal ion removal process. Ion exchange was found to be the main pathway through which metal ions were stripped away.[8] When the Ca-type resin (CABIER) is immersed in an acid, calcium ions can be replaced by hydrogen ions according to the following reaction:

$$2H^+ + [CaR] = Ca^{2+} + [H_2R] \quad (1)$$

Similarly, in an aqueous solution of metal salts, exchange between metal ions and calcium ions inside the resin takes place:

$$M^{2+} + [CaR] = Ca^{2+} + [MR] \quad (2)$$

A greater affinity of R^{2-} to M^{2+} is the driving force for pushing the equilibrium to the right.

In addition, there may be some "free/unreacted" functional groups in the fresh CABIER, leading to the formation of an ion-pair ($M^{2+}R^{2-}$):

$$M^{2+} + R^{2-} = [MR] \quad (3)$$

In addition, precipitation and aqueous solution reactions were considered according to refs 14,18. It was assumed that a metal-containing system had M_x aqueous species with concentrations x_i, and M_p precipitated species with activities of unity. One can describe the concentrations or activities of the two types of species in terms of N_a aqueous components with concentrations c_j. The equilibrium

(18) Schecher, W. D.; McAvoy, D. C. *MINEQL+ Chemical Equilibrium Modeling System*, version 4.5 for Windows; Environmental Research Software: Hallowell, ME, 2001.

Table 1. Chemical Reactive Properties in Metal Binding

no.	reaction	K	PIB[a]	ionic radius[b,c]
a	$2H^+ + R^{2-} \rightarrow H_2R$	$10^{8.000}$ M^{-2}	0	
b	$Ca^{2+} + R^{2-} \rightarrow CaR$	$10^{5.657}$ M^{-1}	0.89	$r_{Ca^{2+}} = 0.78$ Å
c	$Pb^{2+} + R^{2-} \rightarrow PbR$	$10^{7.257}$ M^{-1}	1.11	$r_{Pb^{2+}} = 0.98$ Å
d	$Cu^{2+} + R^{2-} \rightarrow CuR$	$10^{6.205}$ M^{-1}	1.02	$r_{Cu^{2+}} = 0.57$ Å
	content of functional group (R^{2-}) = 3.338×10^{-3} mol/g			$r_{-CO_2^-} \cong 2.25$ Å

[a] Frequencies of the asymmetric vibration of the carboxylate group were obtained from Figure 9: $\nu_{(CO_2H)} = 1740$ cm^{-1}; $\nu_{(CO_2Na)} = 1619$ cm^{-1}; $\nu_{(CO_2Ca)} = 1632$ cm^{-1}; $\nu_{(CO_2Pb)} = 1606$ cm^{-1}; $\nu_{(CO_2Cu)} = 1617$ cm^{-1}. [b] The radius of the carboxylate anion is obtained from the radius of the acetate anion (CH_3-CO_2-) by deducting the size of the CH_3 group. [c] Ref 25.

relationships that give the concentrations or activities of the two types of species are

$$x_i = K_i^x \prod_{k=1}^{N_a} c_k^{a_{ik}{}^x} \qquad i = 1, 2, ..., M_x \tag{4}$$

$$K_i^p \prod_{k=1}^{N_a} c_k^{a_{ik}{}^p} = 1 \qquad i = 1, 2, ..., M_p \tag{5}$$

where K_i^x denotes the equilibrium constant of the ith aqueous species; a_{ik}^x, the stoichiometric coefficient of the kth aqueous component in the ith aqueous species; K_i^p, the modified equilibrium constant of the ith precipitated species; a_{ik}^p, the stoichiometric coefficient of the kth aqueous component in the ith precipitated species.

On the basis of the above equations and mass balances, the distribution of ions in both solid and liquid phases can be easily obtained by using such equilibrium models as the *MINEQL+*[18] and *FITEQL 4.0*.[19] As the CABIER was a newly developed material, there was no information available in the literature on these reactions (eqs 1 to 3) and their equilibrium constants. Therefore, a series of titration and adsorption isothermal experiments had to be carried out to provide input data for the model.

As analytical solutions to the above equations were difficult to obtain, the computer program of *FITEQL 4.0* could be used. Slight changes in the above equations had to be made because [CaR] could not be treated as a component (according to the *FITEQL 4.0* requirements) and the "free/unreacted" functional groups (R^{2-}) were present. The resulting reactions are listed in Table 1. A slight rearranging of the reactions will yield the above eqs 1 and 2.

Calibration of the Model. Titration data were used to determine the content of functional groups and the reaction constants of eqs a and b in Table 1. Sorption isotherms were obtained to provide data to determine the equilibrium constant(s) of eqs c and d. After the determination of all reaction constants, prediction of metal removal under other conditions could be performed.

Results and Discussion

Equilibrium Experimental Study. Acid-titration experiments were performed with the results shown in Figure 1. The solution pH decreased with an increasing concentration of nitric acid. The functional groups (i.e., CaR and R^{2-}) consumed hydrogen ions according to the hypothesis presented in the Theoretical Section. The ionic strength effect appears less important as illustrated (i.e., 0.05 M versus 0.1 M), indicating that the ionic strength effect on hydrogen consumption could be neglected.

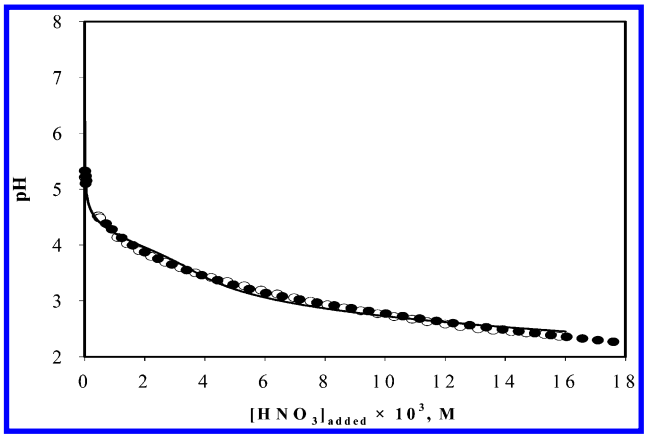

Figure 1. Titration of CABIER. Condition: $NaNO_3$ added as ionic strength, m = 5 g/L, $[HNO_3]_o$ = 0.1 M. Illustration: ● experimental (I = 0.05 M), ○ experimental (I = 0.1 M), − modeling.

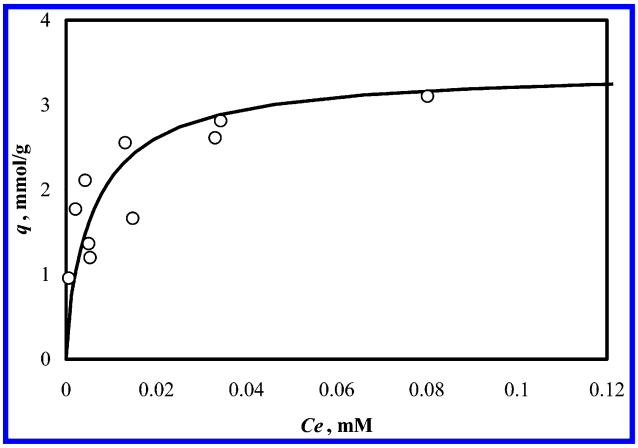

Figure 2. Lead sorption isotherm. Illustration: ○ experimental, − modeling.

The adsorption isotherm of lead(II) is illustrated in Figure 2. Metal removal capacity (q, mmol/g) is defined as the amount of metal removed (mmol) per mass of the resin (g), while C_e is the equilibrium metal concentration (mM). The results show that the metal adsorption capacity by the resin is significantly higher than that by commercially available activated carbons. Normally, activated carbons can adsorb heavy metal ions of 0.05 to 0.15 mmol-metal/gram-carbon. However, the adsorption capacity of the CABIER can be as high as 3 mmol-Pb/gram-CABIER (Figure 2). Figure 3 shows that the removal capacity increases with pH within a certain range: pH = 3 is sufficient for a complete uptake of lead, while the highest removal of copper is achieved at pH 4. From an engineering standpoint, the resin is more suitable for lead removal.

(19) Herbelin, A.; Westall, J. *FITEQL: A Computer Program for Determination of Chemical Equilibrium Constants from Experimental Data, Version 4.0*; Technical Report. Department of Chemistry, Oregon State University, Corvallis, OR, 1999.

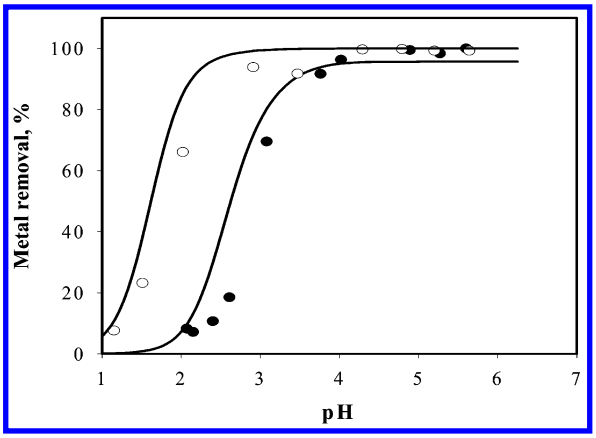

Figure 3. pH effect on metal removal. Condition: $[Pb]_o = 1.0 \times 10^{-4}$ M, $m = 1$ g/L, $[Cu]_o = 1.0 \times 10^{-4}$ M, $m = 0.15$ g/L. Illustration: ● experimental (Cu), ○ experimental (Pb), − modeling.

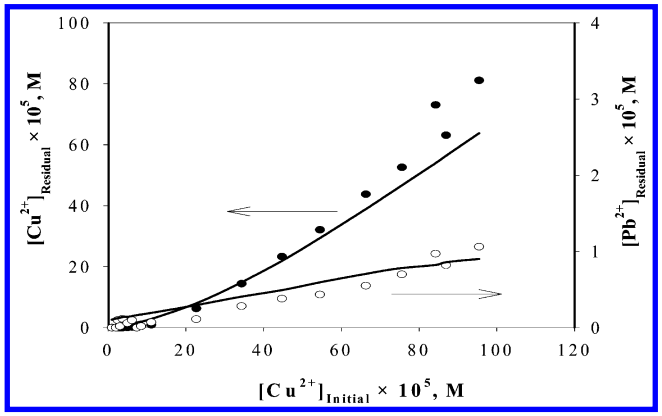

Figure 4. Effect of copper concentration on bimetal removal. Condition: pH = 5.5−7.0, $m = 0.167$ g/L, $[Pb]_o = 1.0 \times 10^{-4}$ M. Illustration: ● experimental, − modeling.

Competitive adsorption experiments of lead and copper were conducted. When the initial copper concentration was increased from 0 to 9.54×10^{-4} M and the lead concentration was maintained at 1×10^{-4} M, the copper residual concentration was also increased from 0 to 8.11×10^{-4} M (see Figure 4). The residual lead concentration, on the other hand, remained below 1.06×10^{-5} M as the resin is favorable to lead removal. When the concentrations of these two metals were similar to each other, more lead ions were removed.

Microscopic Studies. *Morphology of Resin*. Samples of resins before and after metal adsorption were observed using the SEM/EDS technique with an aim to identify the surface microstructures and determine the chemical composition. The SEM images of the resin in Figure 5a−c showed less pore development occurring in the resins.

Figure 5a shows the approximate dimensions of the fresh resin particles; the morphology of surface matrix of the dried resin is displayed in Figure 5b. An interesting observation is the alteration of surface morphology after Ca^{2+} ions are replaced by Cu^{2+} ions (Figure 5c). A less rugged surface is observed, which can be due to the difference in the coordination sphere of these two metal ions. Cu^{2+} offers a smaller coordination sphere than Ca^{2+}, since Cu^{2+} has a smaller ionic radius than Ca^{2+} (see Table 1). On average, the coordination sphere of Cu^{2+} embraces a smaller number of −OH and $-COO^-$ groups than that of Ca^{2+}. As a result, the polymer chains become less twisted or folded in the Cu^{2+}-bound matrix.

As shown in Table 2, the surface compositional measurement (atomic %) of the two different resins by the EDS is inconsistent. For the fresh resin, the atomic ratio of C/O equals to 1.07, which is almost the same as that of alginate (molecular formula of $C_{13}O_{12}$). However, this ratio increases to 1.29 for the Cu^{2+}-adsorbed resin, implying that the polymer matrix becomes softer after the ion exchange. The oxygen-containing polar groups are able to retreat from the surface in order to lower the surface energy during the drying process, since polysaccharide chains are flexible in the wet state. This interpretation is consistent with the change in surface morphology due to the adsorption of Cu^{2+} ions (Figure 5c).

As illustrated in Table 2, the calcium atomic % on the resin surface decreases while the copper atomic % increases, indicating the copper uptake mechanisms of the ion exchange (between Ca^{2+} and Cu^{2+}) and the coordination (Cu^{2+} with organic functional groups). On the basis of our previous study[8] as well as the instrumental analysis discussed later in this paper, it is found that the copper removal is mainly due to the ion exchange. However, the decrease in the calcium atomic % in the resin is higher than the increase in the copper atomic % (Table 2). This inconsistent observation is due to the limitation of the EDS since it can only determine the elemental compositions on the surfaces.[20]

X-ray Photoelectron Spectroscopy. XPS was employed to study the shifts of binding energy (BE) of the respective coordination atom (oxygen O1s) and its neighboring atom (carbon C1s) in various samples with the results shown in Figure 6a−b.

The C 1s spectrum of sample *d* comprised three peaks with BE of 285.8, 287.2, and 288.9 eV identified via the deconvolution (Figure 6a). These peaks can be assigned by following the above sequence, to ether, alcoholic,[21] and carboxylate groups,[21,22] which represent the three different chemical surroundings of carbon atoms in the polymer backbone of sodium alginate (Figure 7). Among them, ether and alcoholic carbons represent the abundant species in the resin.

Furthermore, it can be observed from spectrum (*a*) that, the peak for the calcium-type resin (*a*) at 287.4 eV dramatically decreases, resulting in a new peak at 290.5 eV. This change is attributed to the participation of the −OH group into the coordination sphere of the Ca^{2+} ion, which is known as a stronger Lewis acid than Na^+ ion. It is logical to associate the new peak at 290.5 eV with the carbon of the coordinated alcohol groups with Ca^{2+} ions.

On the basis of the above observations and discussions, it is not difficult to understand the increase in the intensity of the peaks at 290.5 eV relative to the other peaks (sample *e* in Figure 6a) when the calcium-type of resin (*a*) was partially protonated. Due to the formation of hydrogen bonding between H^+ and −OH, the resultant $-OH_2^+$ group loses coordination ability with Ca^{2+}. Comparison of spectra (*b*) and (*c*) in Figure 6a shows that the free alcohol groups in sample *b* are more abundant than those in sample *c*. It suggests that the Cu^{2+} adsorption requires the involvement of more alcoholic groups. The fundamental chemistry also supports this explanation, since the Cu^{2+} ion has a d^9 valence configuration and has been known to accommodate, in its coordination sphere, 4 or 6 coordination atoms, whereas the Pb^{2+} ion normally accepts only 2. More importantly, the XPS assignment is coherent with the experimental results shown in Figure 3. The removal

(20) Karatza, D.; Lancia, A.; Musmarra, D.; Zucchini, C. *Exp. Thermal Fluid Sci.* **2000**, *21*, 150−155.
(21) Polovina, M.; Babic, B.; Kaluderovic, B.; Dekanski, A. *Carbon* **1997**, *35*, 1047−1052.
(22) Pakula, M.; Biniak, S.; Swiatkowski, A. *Langmuir* **1998**, *14*, 3082−3089.

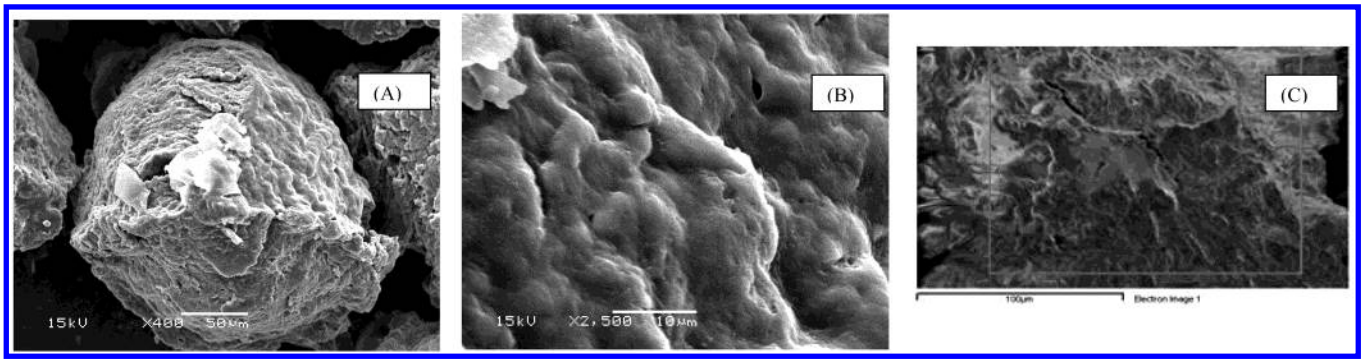

Figure 5. SEM micrographs of CABIER: (a) fresh CABIER (×400); (b) fresh CABIER (×2500); (c) Cu-adsorbed CABIER (×200).

Table 2. Composition (atomic %) Obtained by the EDS Microanalysis of the Resins

resins	O	C	Ca	Cu
fresh	48	51.3	0.5	
Cu^{2+}-adsorbed	42	54.2	0.1	3.5

capacity of Pb^{2+} was greater than that of Cu^{2+} at pH < 2, because the protonation of the hydroxyl group in an acidic medium impeded the coordination ability of the −OH group.

Three O1s peaks are identified after deconvolution, which come from the different groups of the resins (Figure 6b). BE peaks of 532.0 and 533.3 eV can be assigned, respectively, to COO^- and C−O−R (ether and alcohol) for sample *d*. These two assignments are reasonable because the ratio of these two peak areas reflects the tratio of the different functional groups in the alginate (molecular formula of $C_{13}O_{12}$). When the Na alginate (sample d) was converted to Ca alginate, a new XPS peak emerged at 534.6 eV in sample *a* (Figure 6b). As this value is beyond the range of BE (O1s), which most organic functional groups could possess, it is tenable to accept this peak as a result of the coordination of hydroxyl groups to metal ions. The O1s spectra of samples *b* and *c* show additional support to previous deduction on the different coordination capacity of alcohol to Pd^{2+} compared to Cu^{2+}: there are more un-coordinated −OH groups in the Pb^{2+}-adsorbed sample than in the Cu^{2+}-adsorbed sample. In addition, the coordinated −OH groups (marked by the peak at 534.6 eV) are more abundant in the Cu^{2+}-adsorbed sample (spectrum *c*) than in the Pb^{2+}-adsorbed sample (spectrum *b*).

Figure 8a−c displays the XPS spectra of elements Ca (2p), Pb (4f), and Cu (2p) for samples *a*, *b*, and *c*, respectively. Ca was not detected on the surfaces of samples *b* and *c*, indicating that most of the Ca^{2+} ions in the fresh CABIER were replaced by Pb^{2+} or Cu^{2+} ions through ion exchange. The peak of Ca $2p_{3/2}$ at 348.7 eV obtained from sample *a* may represent the bonding O−Ca−O (Figure 8a). The same BE was found in $Ca(NO_3)_2$.[23] Similarly, the peak of Pb (4f) for sample *b* at 137.0 eV in Figure 8b was due to the formation of O−Pb−O bonding with a reference to the assignment for $Pb(OH)_2$.[24] The fact that multi-valence metal ions (e.g., Ca^{2+}) combine with two or more oxygen-containing groups (e.g., $-COO^-$ or −OH) would lead to a cross-linking effect when a mono-valence counterion (e.g., Na^+) in the resin is replaced by them. This effect causes the matrix of the adsorbent to become more compact and water-insoluble.

As far as the adsorption of Cu^{2+} on the CABIER is concerned, there are two sets of Cu core-level XPS spectrum ($Cu_{2p3/2}$ and $Cu_{2p1/2}$). In view of 2p3/2 spectrum, it could be fit by two peaks with binding energy of 932.8 and 935.0 eV. Chen et al.[25] reported that the first peak of 932.8 eV was characterized as the alginate-bound Cu^{2+}. The second peak (935.0 eV) originated from Cu^{2+} located in the coordination sphere different from the former one. According to the two different peak areas, the first type of coordination sphere is a prevalent one in comparison to the second type. It is rational to presume that the first type of coordination sphere contains four ligands while the second one has six ligands.

Fourier Transform Infrared Spectroscopy. The FT-IR spectra of the five samples (*a*−*e*) defined previously are compared in Figure 9. The Na alginate (sample *d*) can be used as a reference, because only the carboxylic group bonds with the Na^+ ion in its matrix. It is clear that carboxylate anion gives rise to two bands: a strong

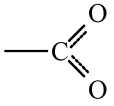

asymmetrical stretching band at 1618 cm^{-1} and a weaker symmetrical stretching band at 1420 cm^{-1}. The broad band at 1083 cm^{-1} is due to the C−O stretching of both alcoholic and ether groups. An interesting phenomenon is the shift of this vibration frequency (from 1083 to 1028 cm^{-1}) when Na^+ is replaced by Ca^{2+} (sample *a*). It happens as a result of the coordination of both alcoholic and ether groups to Ca^{2+} ion, which weakens the C−O bond strength in these two functional groups. The same interaction also took place in sample *b* (Pb^{2+} as the counterion) and in sample *c* (Cu^{2+} as the counterion). Another noticeable feature is that the C−O band of sample *b* has a greater frequency and is broader than the corresponding band of sample *c*. This structural message supports the above inference (based on the XPS analysis), in which the adsorption of Cu^{2+} is considered to involve more alcoholic groups than that of Pb^{2+}. The shape of the C−O band of sample *c* (at 1027 cm^{-1}), which is narrower and sharper compared to the same type of band in the other spectra, could be linked with orthodox coordination spheres,[26] wherein all oxygen−Cu bonds have a very similar strength. In all the spectra, except spectrum *e*, the double bands of the carboxylate anion as aforementioned are identical with the observation made by Figueira et al.[24]

After CABIER (sample *a*) was partially protonated via HNO_3 titration, sample *e* could be obtained. Its spectrum

(23) Moulder, J. F.; Stickle, W. F.; Sobol, P. E.; Bomben, K. D. *Handbook of XPS*; Physical Electronics Division: Perkin-Elmer Corporation, 1992.

(24) Figueira, M. M.; Volesky, B.; Mathieu, H. J. *Environ. Sci. Technol.* **1999**, *33*, 1840−1846.

(25) Chen, X.; Guan, H.; Su, Y. *J. Inorg. Organomet. Polym.* **2000**, *10*, 115−126.

(26) Banerjea, D. *Coordination Chemistry*; McGraw-Hill: New Delhi, 1997.

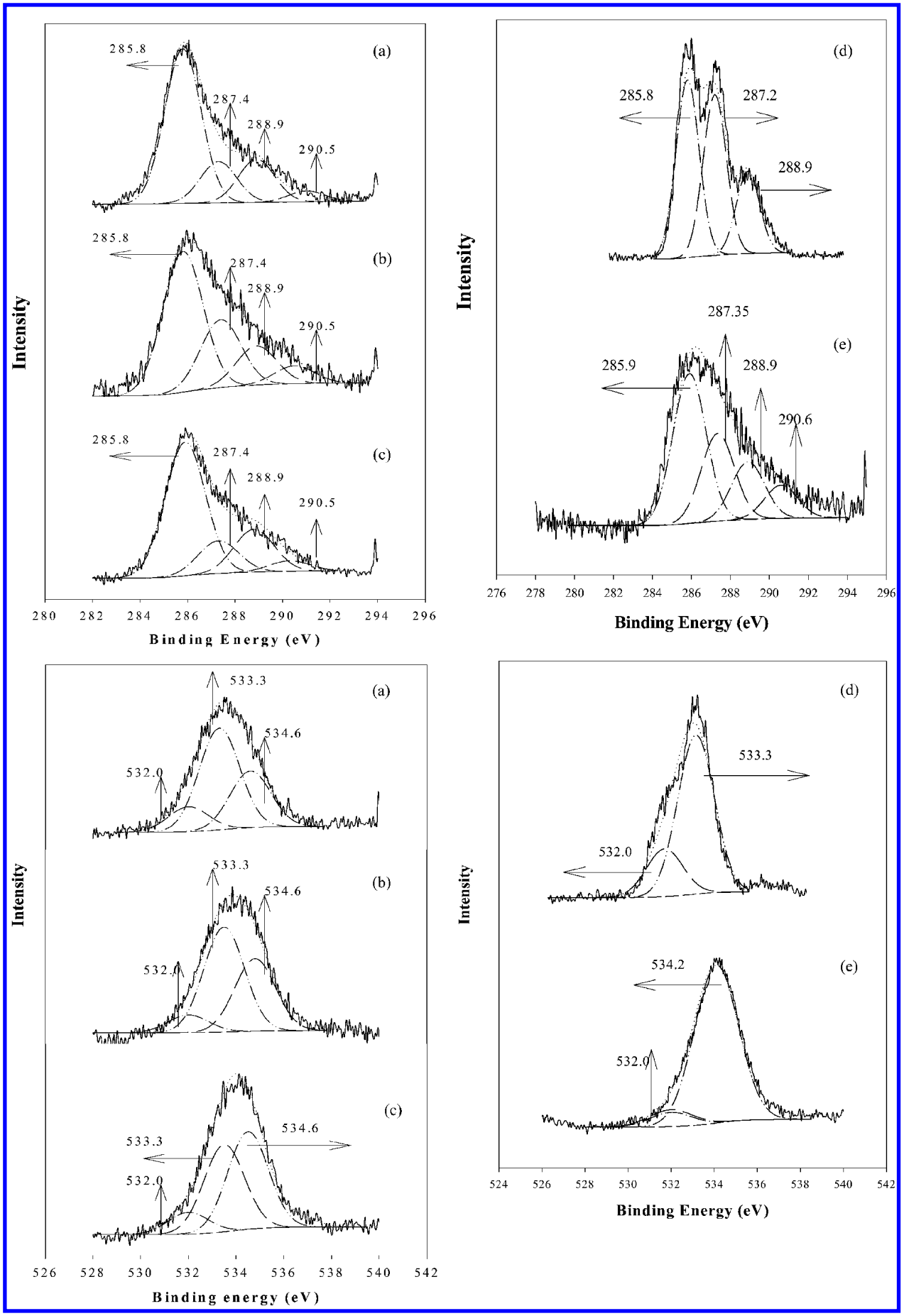

Figure 6. XPS spectra of the resins: (a) Cls, top; (b) Ols, bottom. Illustration: *a*: fresh resin; *b*: Pb-adsorbed resin; *c*: Cu-adsorbed resin; *d*: Na alginate powder; *e*: acid-titrated resin.

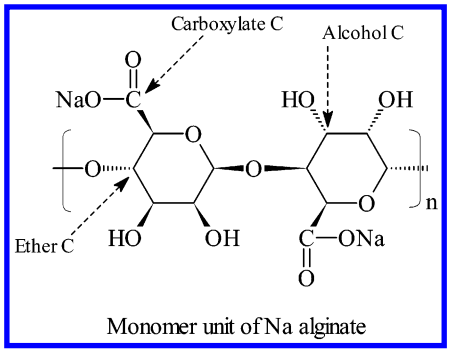

Figure 7. Proposed molecular structure of alginate.

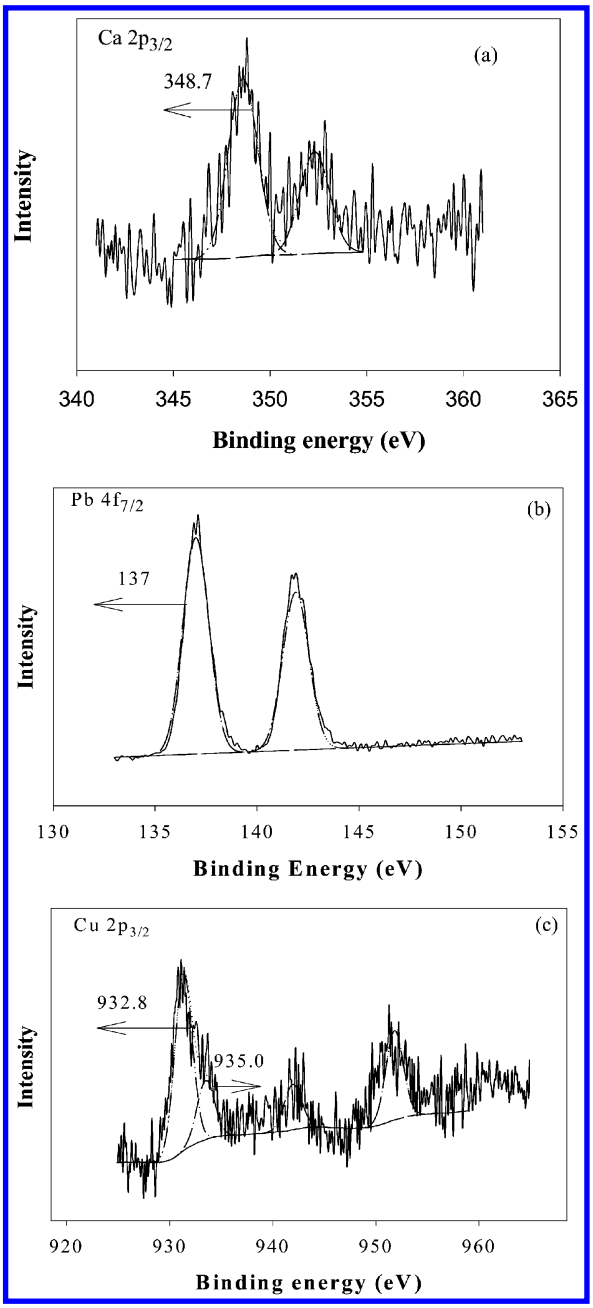

Figure 8. XPS spectra of CABIER: (a) fresh resin; (b) Pb-adsorbed; (c) Cu-adsorbed.

exhibits two types of C=O absorption bands at 1740 and 1632 cm^{-1}. The origin of the former peak is not clear, because its frequency is higher than that of carboxylic acid, C=O. One possibility is the formation of an ester group that has the C=O frequency in the region of 1755−1740 cm^{-1}. This means that carboxylic acid groups generated from the acidification of calcium carboxylate reacted with alcoholic groups (i.e. esterification) under the catalysis of acid. The 1632 cm^{-1} peak is due to an un-acidified carboxylate anion. Furthermore, a sharp and strong peak appearing at 1385 cm^{-1} is the distinct feature of spectrum *e*. This peak could be attributed to the bending mode of C−O−H that occurs in an alcoholic group, a protonated alcoholic group, and a protonated ether group. The high intensity of this peak gives an indication that the major acidification site is C−O−R (R = H or C). In conclusion, the FT-IR study in the five kinds of samples further ascertains the chemistry of the functional groups in the resins.

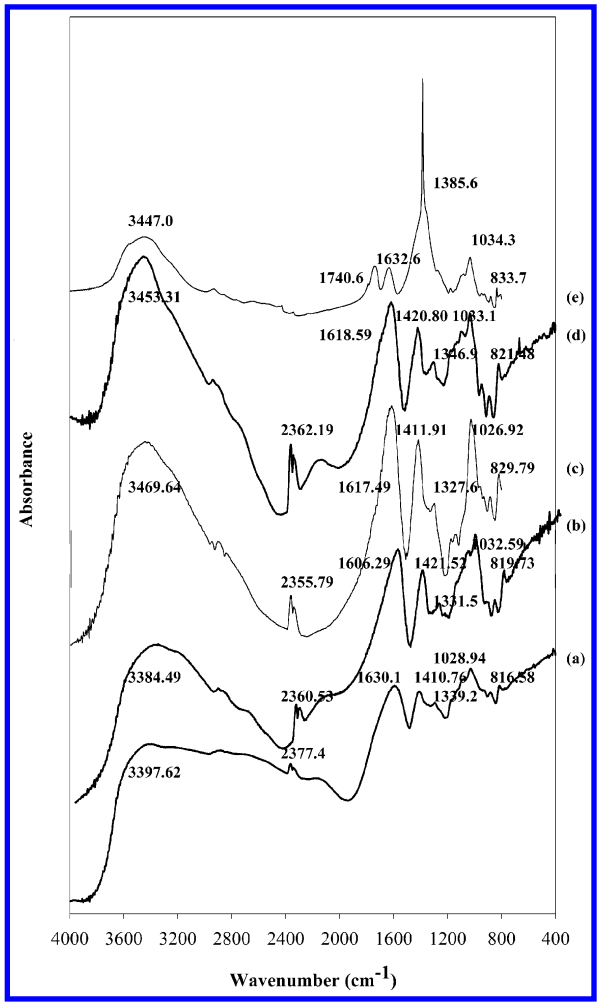

Figure 9. FT-IR spectra of the resins: (a) fresh resin; (b) Pb-adsorbed resin; (c) Cu-adsorbed resin; (d) Na alginate powder; (e) acid-titrated resin.

Modeling. *Determination of Functional Group Content and H− and Ca−R Constants.* According to the approaches stated in the *Theoretical Section*, the titration data (ionic strength of 0.1 M) were used for the determination of the content of functional groups and the equilibrium constants for reactions a and b in Table 1. The calcium concentration (based on a digestion experiment) used in the modeling (*FITEQL 4.0*) was 3.0×10^{-3} mol/g.[8] Aqueous solution reactions among Ca^{2+}, H^+, and OH^- were also included.

The simulation based on the reactions and experimental data was performed with the results shown in Figure 1 and Table 1. The model provided an excellent representation of the titration data. On the basis of reactions a and b, the reaction constant of eq 1 discussed in the Theoretical Section is $10^{2.343}$ M^{-1}.

The content of functional groups was found to be 3.338 $\times 10^{-3}$ mol/g, slightly higher than that of calcium (3.0×10^{-3} mol/g).[8] As discussed in the Theoretical Section, it was assumed that calcium was exchanged by copper and lead uptake. At the same time, additional metal removal was due to the reactions with the "free" functional groups in the resins. The content difference between Ca^{2+} and R^{2-} based on this calculation confirms our assumption. The ratio between Ca^{2+} and R^{2-} was therefore fixed at 0.9:1.0 in subsequent calculations. The functional group content of 3.338×10^{-3} mol/g indicates the limitation of maximum metal uptake capacity.

Determination of M−R Constants. Determination of the constants of reactions c and d in Table 1 was subsequently conducted based on the lead and copper adsorption isothermal data. These reactions, together with precipitation and aqueous solution reactions due to the presence of Ca^{2+}, Pb^{2+}, and Cu^{2+}, were included in the modeling. The precipitation and aqueous reaction constants were obtained from the database in *MINEQL+*.[18]

Figure 2 shows that the model well represented the lead isothermal data (copper not shown here). On the basis of reactions (b), (c) ,and (d), the reaction constants of eq 3 discussed in the Theoretical Section are $10^{1.6}$ and $10^{0.548}$ M^{-1} for lead and copper binding, respectively. The sequence of the constants shows that the resin removes lead preferentially.

As shown in Table 1, the equilibrium constants of metals follow a descending order of PbR > CuR > CaR. In light of the fact that the carboxylate group in the alginate resin played an important role in binding metal ions, percentage of ionic bonding (PIB) was defined:

$$\mathrm{PIB} = \frac{\nu_{(CO_2H)} - \nu_{(CO_2M)}}{\nu_{(CO_2H)} - \nu_{(CO_2Na)}} \qquad (6)$$

where ν is the frequency of the asymmetric vibration of the carboxylate group.

In the formula of PIB, the denominator is the IR frequency shift of the asymmetric C═O vibration from the typical covalent bonding (carboxylic acid) to the typical ionic bonding (sodium carboxylate), whereas its numerator term is the frequency shift of the same vibration when a particular metal ion is bound.

On the basis of the frequencies measured from the FT-IR analysis (Figure 9), PIB was calculated. It is interesting to find that the PIB values in Table 1 are coincident with the sequence of the *K* values of the three metal ions. In the cases of Pb^{2+} and Cu^{2+}, their PIB values are greater than unity, which is caused by their lower carboxylate vibration frequencies than the case of Na carboxylate. This occurrence can be interpreted as a decrease in the electron density at the carboxylate group as a result of electron delocalization. The electron delocalization could be attributed to polarization or electron feedback-bonding between a metal ion and a carboxylate group. In general, the electron delocalization effect is beneficial to the metal−carboxylate binding, which has been also supported by the sequence of the *K* values.

Prediction of Effects of pH and Competing Metals. The parameters discussed above were obtained by the optimization techniques. From a mathematical standpoint, there may be more than one set of parameters that are able to represent experimental data. The model may not be so accurate when applied to cases under different operational conditions. To test the applicability of the model, the pH effect on the metal removal was predicted by the reactions in Table 1. The experimental conditions, such as initial metal concentration and resin amount were used as input to the model.

Prediction of pH effect on metal removal was first performed. As shown in Figure 3, the model successfully describes the pH effect on both lead and copper uptake. The competition in the metal removal (i.e., Cu−Pb uptake) was then predicted as shown in Figure 4. Once again, the model in most cases predicted well the bimetal removal.

The simulation of single-component adsorption equilibrium by simple adsorption isotherm equations has been well documented. Modeling of multicomponent adsorption, however, still remains challenging to many researchers. A series of empirical/semiempirical models have been documented in various studies, e.g., extended Langmuir equation, extended Langmuir-Freundlich equation, and ideal adsorbed solution theory.[27] However, not many successful applications have appeared in the literature. An early study done by Benjamin and Leckie[28] probably is one of very few studies. In our earlier study, an extended Langmuir equation was used to simulate the removal process. The modeling results unfortunately were far away from the experimental observations, particularly for the copper removal in the Pb−Cu case (Figure 4).

One can see that a complicated multiple-metal-ion adsorption process can be elucidated on the basis of a combination of simple single-metal-ion removal reactions. This is the major advantage of the developed model over other empirical/semiempirical models. It has to be pointed out that there was some disagreement between the predicted and observed values. This somewhat poor description was due to inaccuracy of the respective single-metal-ion adsorption reactions (e.g., Figure 2). Meanwhile, as the system contains more types of metal ions, the error between the calculated and observed values could increase.

Some Comments on Microscopic Observations versus Mathematical Modeling. The mathematical models for the description of metal uptake processes (e.g., sorption and ion exchange) have traditionally been developed on various assumptions (e.g., surface complex formation and ion exchange), which essentially result from the macroscopic observations (e.g., measurements of contaminant concentrations and pH). The results of the modeling simulation, however, are parameter-dependent. Hence, there can be a gap between the modeling results and experimental data.

In recent years, microscopic measurements by various state-of-the-art instruments, such as XPS, SEM, and FT-IR, attract more attention as they can provide realistic information of the environmental processes from the microscopic viewpoints. There are many interesting findings appearing in the literature on metal adsorption and biosorption processes (e.g., refs 24,29). For example, Dambies et al.[29] used XPS study of chemical interactions between Cu(II), Mo(VI), and Cr(VI) and chitosan. A series of complicated chemical reactions (e.g., adsorption and reduction) was involved in the removal of the metals.

These techniques, however, can provide only a qualitative analysis of the processes. With the findings from these studies together with mathematical modeling simulations (quantitative analysis), one therefore can describe the environmental phenomena more accurately and subsequently predict the removal capacities under various operational conditions.

(27) Tien, C. *Adsorption calculations and modeling*; Butterworth-Heinemann: Boston, MA, 1994.

(28) Benjamin, M. M.; Leckie, J. O. *J. Colloid Interface Sci.* **1981**, *83*, 410−419.

(29) Dambies, L.; Guimon, C.; Yiacoumi, S.; Guibal, E. *Colloid Surf., A* **2001**, *177*, 203−214.

Conclusions

Copper and lead removal by the CABIER increased with an increasing pH. The metal uptake capacity was much higher than commercially available adsorbents. The SEM images of the resin showed less pore development occurring in the resins. The presence of divalent metals (e.g., Ca and Cu) affected the surface morphology of the resin. The functional groups (i.e., C−O−R and COO^-) played a key role in the removal. The nature of lead uptake was the typical ion exchange between Ca^{2+} and Pb^{2+} at carboxylate anionic site, whereas the copper abstraction took place through the ion exchange between Ca^{2+} and Cu^{2+} as well as the formation of coordination complex (i.e., CuR). A new model considering both ion exchange and coordination reactions successfully simulated the metal removal process under various conditions (e.g., pH and presence of completing metals). The equilibrium constants of metal stripping obtained by the modeling reveal a decreasing order of $Pb^{2+} > Cu^{2+} > Ca^{2+}$, which is the same as the bonding strength order between metal and carboxylate group derived from the FT-IR analysis.

Acknowledgment. The financial support provided to J.P.C. by the National University of Singapore under R-279-000-104-112 is appreciated.The authors thank Dr. Simo Olavi Pehkonen (Department of Chemical and Environmental Engineering, NUS) for his valuable comments on this manuscript.

Note Added after ASAP Posting

This article was released ASAP on 10/25/2002 with an error in equation 5. The correct version was posted on 11/05/2002.

LA026060V